Electronic Supplementary Information (ESI) for

In situ formation of hole transporting material on bismuth tungstate for innovative photoelectrochemical aptasensing

Tianli Liu, Mengmeng Gu, Lingling Zhao, Xiuming Wu, Zaijun Li, and Guang-Li Wang*

Key Laboratory of Synthetic and Biological Colloids (Ministry of Education), School of Chemical and Material Engineering, Jiangnan University, Wuxi 214122, China

Corresponding author:

* E-mail: glwang@jiangnan.edu.cn

Experimental Section

Materials and Chemicals. $Bi(NO_3)_3 \cdot 5H_2O$, $Na_2WO_4 \cdot 2H_2O$, potassium ferrocyanide ($K_4[Fe(CN)_6]$), tetraethyl orthosilicate (TEOS) and cetyltrimethylammonium bromide (CTAB) were obtained from Sinopharm Chemical Reagent Co., Ltd. (Shanghai, China). Chloramphenicol (CAP), 3-aminopropyltriethoxysilane (APTES) and oligonucleotides (HPLC-purified) were bought from Sangon Biotechnology Co., Ltd. (Shanghai, China). The sequence of the oligonucleotides used is listed as follows: The CAP aptamer: 5′-ACT TCA GTG AGT TGT CCC ACG GTC GGC GAG TCG GTG GTA G-3′

Instrumentation. Scanning electron microscopy (SEM) images and energy-dispersive X-ray (EDX) mapping were determined by a Hitachi S-4800 high resolution scanning electron microscope equipped with an EDX detector (Hitachi, Japan). Transmission electron microscope (TEM) images were determined by a JEM-2100 plus transmission electron microscope (Japan). The X-ray diffractometer (XRD) pattern was determined by an X'Pert Philips materials research diffractometer (Brook AXS, Germany). UV-vis absorption spectra were determined by a UV-3600 plus UV-vis Spectrophotometer (Shimadzu, Tokyo, Japan). Fluorescence spectra were measured on a Cary Eclipse fluorescence spectrophotometer (Varian Co. Ltd., USA). Cyclic voltammetry (CV), differential pulse voltammetry (DPV), electrochemical impedance spectroscopy (EIS), and photocurrent measurements were carried out on a CHI 800C electrochemical workstation (Shanghai Chenhua Instrumission, China). The surface photovoltage (SPV) spectroscopy was measured by PL-SPS1000 surface photovoltage spectrometer (Changchun, China).

Preparation of the Bi_2WO_6 and its modification on the ITO electrode. The hydrangea Bi_2WO_6 was prepared according to the previously reported hydrothermal method.[1] Firstly, 0.98 g of $Bi(NO_3)_3 \cdot 5H_2O$ was added to 40 mL of 0.3 M HNO_3 and dissolved under ultrasound. Then, 20 mL of 0.05 M $Na_2WO_4 \cdot 2H_2O$ solution was added under vigorous stirring, producing a white precipitate. After that, 20 mL of 0.2 M NaOH solution was added dropwise and then stirred for another 24 hours. Subsequently, the mixture was transferred to an autoclave, and heating was continued at 160 °C for 8 hours. After the reaction was completed, it was cooled to room temperature naturally. The obtained suspension was centrifugally washed with deionized water and absolute ethanol for several times. Finally, the centrifuged product was dried in an oven at 60 °C overnight to obtain the Bi_2WO_6 powder. The Bi_2WO_6 powder was ultrasonically dispersed in deionized water to prepare a 1.0 mg/mL suspension. Pipette 28 μL of the Bi_2WO_6 suspension droplets on the surface of the cleaned ITO electrode (with an effective working area of 0.25 cm^2) and then put it in a 40 °C oven for drying to finally obtain the Bi_2WO_6 modified ITO (Bi_2WO_6/ITO) electrode.

Synthesis of positively charged, amine modified mesoporous silica (PMSN). Mesoporous silica (MSN) was synthesized under alkaline reaction conditions according to the previously reported synthesis method by using cetyltrimethylammonium bromide (CTAB) as the pore-forming agent and tethyl orthosilicate (TEOS) as the silicon source.[2,3] Specifically, 1.0 g of CTAB was dissolved in 480 mL of deionized water. Then, adding 3.5 mL of 2.0 M sodium hydroxide to the CTAB solution under magnetic stirring and heat to 70 °C. Subsequently, 5.0 mL of TEOS was dropped into the CTAB solution at a rate of 1.0 mL/minute, and the mixture was vigorously stirred at 80 °C for 6 hours to obtain a white flocculent precipitate to obtain crude MSN. Then, it was washed with ethanol and deionized water alternately 3 times, and the centrifuged product was dried in a 60 °C oven for 4 hours. To remove the excess surfactant in the crude MSN sample, it was calcined in a muffle furnace at 550 °C for 6 hours.

Next, the synthesized MSN is subjected to surface amination treatment.[4,5] A 50 mg of MSN was dispersed in 5 mL of ethanol and sonicated for 2 hours. Then, 1 mL of (3-aminopropyl)triethoxysilane (APTES) was added and stirred at room temperature for 8 hours. Finally, the sample was washed alternately with absolute ethanol and water to remove excess amine, and then placed in an oven at 60 °C to obtain a positively charged amine functionalized MSN (i.e., PMSN).

Homogeneous PEC detection platform for CAP. Before conducting the experiment, the chloramphenicol (CAP) aptamer was heated at 90 °C for 10 minutes, and then slowly cooled to room temperature to release the intermolecular force. A 50.0 mg of PMSN was mixed with 5.0 mL of 0.1 M $K_4[Fe(CN)_6]$ solution and incubated overnight at room temperature with gentle shaking. During this process, $K_4[Fe(CN)_6]$ entered the pores of PMSN through diffusion. Next, 50 μL of CAP aptamer (50 μM) was added to the above reaction solution, and incubated with shaking at room temperature for 4 hours. After the incubation was completed, the final reaction solution was centrifugally and the solids were washed with 10 mM Tris-HCl buffer (pH=7.4) at 3,000 rpm for 5 times to completely remove the unloaded $K_4[Fe(CN)_6]$ and unadsorbed CAP aptamer. The aptamer-coated PMSN loaded with $K_4[Fe(CN)_6]$ at the bottom of the centrifuge tube was resuspended in 5.0 mL of 10 mM Tris-HCl buffer (pH=7.4, containing 0.1 M NaCl) for the subsequent reaction. A 10 μL of the analyte CAP with different concentrations was mixed with 190 μL of the aptamer-coated PMSN loaded with $K_4[Fe(CN)_6]$ in a 96-well microplate, and incubated for 4 hours with shaking at 37 °C. After the reaction, centrifuging the reaction solution, 30 μL of the supernatant was dropwise to the surface of the Bi_2WO_6/ITO electrode and incubated for 5 minutes, and thoroughly washed the electrode surface with deionized water. The PEC measurement was conducted using the LED lamp with wavelength of 370~380 nm as the excitation source, a three-electrode electrode system consisting of Bi_2WO_6/ITO working electrode, Ag/AgCl

reference electrode, and Pt wire counter electrode for recording the photocurrent in 2.0 mL of 0.1 M Tris-HCl solution (pH=7.0) as supporting electrolyte.

Real sample analysis. Local lake water (taken from Lihu Lake, Wuxi) and milk purchased from local supermarket were selected as the real samples for analysis, and pre-treatment was performed before samples analysis. The lake water was first filtered with filter paper to remove suspended solids. Subsequently, the microorganisms were further filtered with a 0.22 μm microfiltration membrane to obtain treated lake water samples. Milk was firstly centrifuged at 10,000 rpm for 10 minutes to remove the upper fat. Subsequently, a 10% volumetric perchloric acid aqueous solution was added to the milk sample to deposit proteins, and then the supernatant was treated with a 0.22 μm microfiltration membrane to obtain a treated milk sample. Next, the pH of the two samples was adjusted with 0.1 M Tris-HCl (pH=7.4). Finally, the treated two samples obtained were stored in a 4 °C refrigerator for use.

Supplementary Results

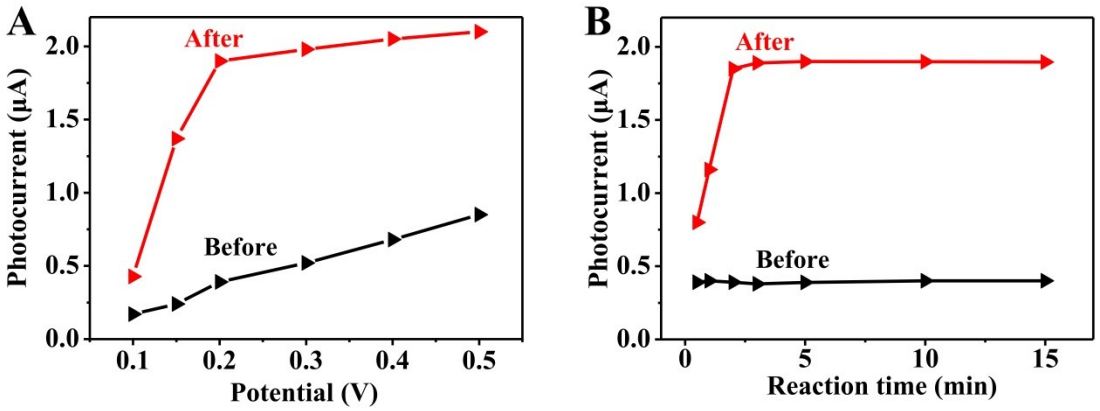

Fig. S1 The effect of (A) applied voltage and (B) reaction time between Bi_2WO_6 and $K_4[Fe(CN)_6]$ on the photocurrent responses of the Bi_2WO_6 modified electrode before (black line) and after (red line) reaction with 0.1 mM $K_4[Fe(CN)_6]$ in 0.1 M Tris-HCl buffer (pH 7.0).

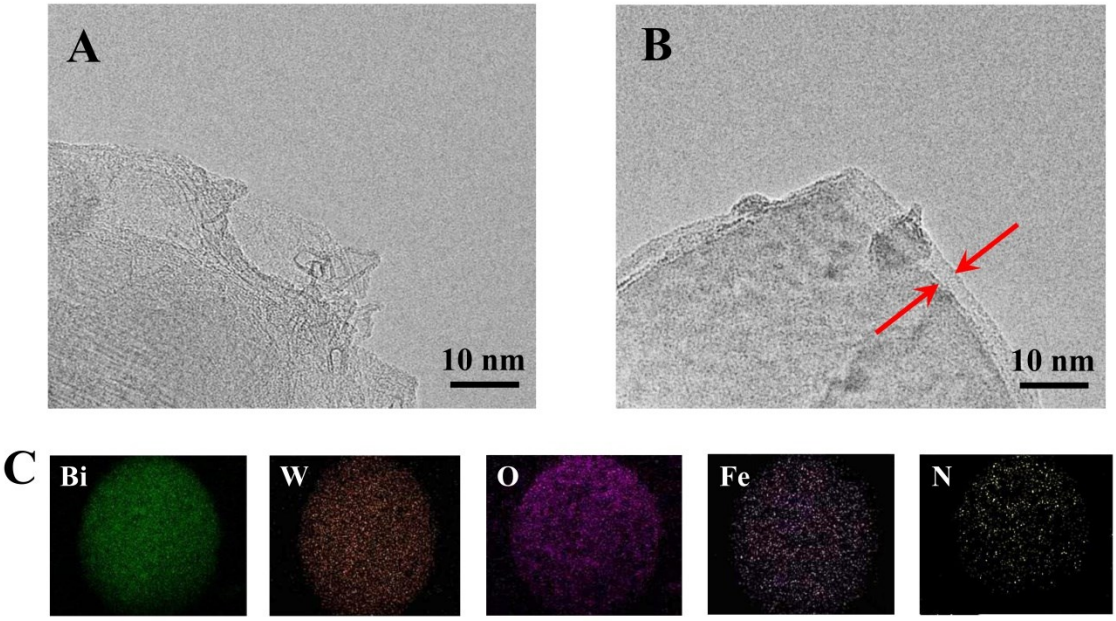

Fig. S2 TEM images of the (A) Bi_2WO_6 and (B) $K_4[Fe(CN)_6]$ treated Bi_2WO_6. (C) EDX elemental-mapping images of $K_4[Fe(CN)_6]$ treated Bi_2WO_6.

According to TEM images (Fig. S2), a thin layer with ca. 2–6 nm thickness was observed for the $K_4[Fe(CN)_6]$ treated Bi_2WO_6 (Fig. S2B), while such layer was not observed in the untreated Bi_2WO_6 (Fig. S2A). EDX mapping (Fig. S2C) revealed that the N and Fe elements were distributed on Bi_2WO_6, confirming the coordination of ferrocyanide to its surface.

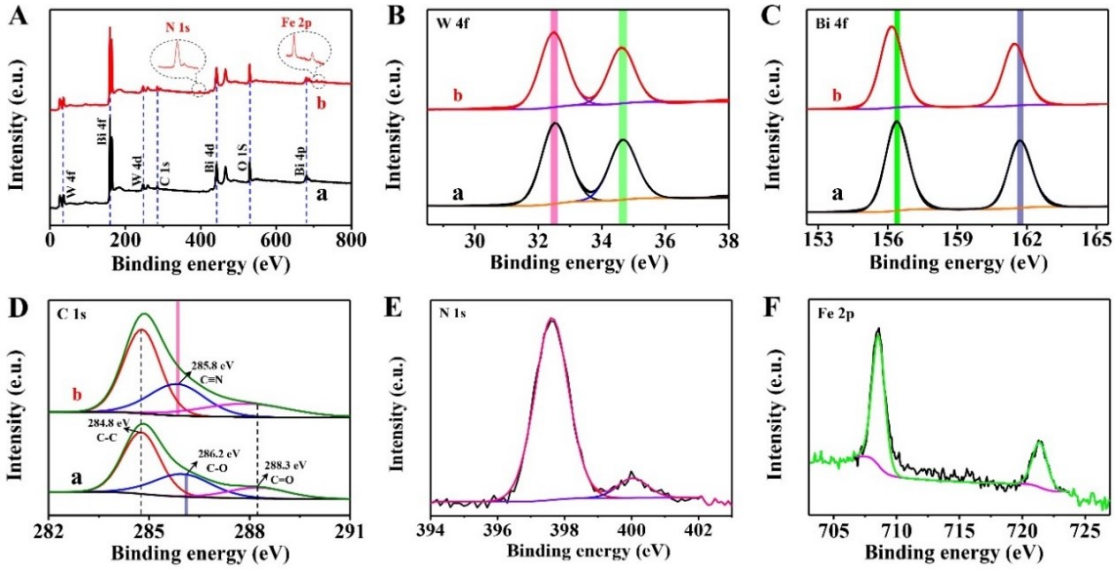

Fig. S3 (A) XPS survey spectra，(B) high-resolution XPS spectra for W 4f, (C) Bi 4f, (D) C 1s of the Bi_2WO_6 (a) and $K_4[Fe(CN)_6]$ treated Bi_2WO_6 (b). High-resolution XPS spectra for (E) N 1s and (F) Fe 2p of $K_4[Fe(CN)_6]$ treated Bi_2WO_6.

The XPS spectra of the untreated and $K_4[Fe(CN)_6]$ treated Bi_2WO_6 samples are demonstrated in Fig. S3. Comparing the survey XPS spectra of pure Bi_2WO_6, two new elements, i.e., N and Fe, were found in $K_4[Fe(CN)_6]$ treated Bi_2WO_6 (Fig. S3A), indicating the conjugation of $[Fe(CN)_6]^{4-}$ to the Bi_2WO_6 surface. For both untreated and $K_4[Fe(CN)_6]$ treated Bi_2WO_6, high-resolution spectra of W 4f had two peaks at the binding energies of 32.5 and 34.7 eV (Fig. S3B), which were assigned to W $4f_{7/2}$ and W $4f_{5/2}$, respectively, and were consistent with the standard value of W(VI). The high-resolution spectrum of Bi 4f revealed two peaks at 156.4 and 161.7 eV (Fig. S3C) that corresponded to the spin states of Bi $4f_{7/2}$ and Bi $4f_{5/2}$, respectively, which was consistent with the literature value of Bi(III) in Bi_2WO_6 sample.[6] In contrast, the peak positions corresponding to Bi $4f_{5/2}$ and Bi $4f_{7/2}$ shifted slightly to lower binding energy for the $K_4[Fe(CN)_6]$ treated Bi_2WO_6, hinting that the conjugation of $[Fe(CN)_6]^{4-}$ to Bi_2WO_6 was closely related to Bi(III). As shown in Fig. S3D of the C 1s spectra, the $K_4[Fe(CN)_6]$ treated Bi_2WO_6 was analyzed by fitting into three carbon types, including the C-C, C≡N and C=O bonds corresponding to binding energies at 284.8, 285.8, and 288.3 eV,[7] respectively. As shown in Fig. S3E, the two binding energies of N 1s were located at 397.6 and 400.0 eV, which were characteristic of N in C≡N.[8] The C≡N bonds were not found in pure Bi_2WO_6, indicating that the C≡N was introduced through the reaction between Bi_2WO_6 and $K_4[Fe(CN)_6]$. Moreover, high resolution scanning spectra also indicated that the Fe(II) element was introduced in the $K_4[Fe(CN)_6]$ treated Bi_2WO_6 (Fig. S3F): The binding energies of 708.6 and 721.3 eV, were respectively corresponding to low-energy spin orbits ($2p_{3/2}$) and high-energy spin orbits ($2p_{1/2}$) of Fe(II).[9]

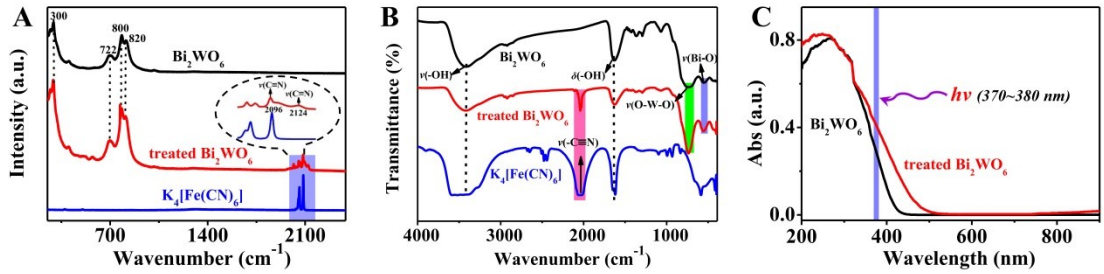

Fig. S4 (A) Raman spectra, (B) FT-IR spectra and (C) UV-Vis DRS of $K_4[Fe(CN)_6]$, Bi_2WO_6 and $K_4[Fe(CN)_6]$ treated Bi_2WO_6.

From the Raman results shown in Fig. S4A, we can see that the band at 722 cm^{-1} was related to the antisymmetric bridge mode of the tungstate chain; bands at 800 and 820 cm^{-1} were the antisymmetric and symmetric Ag modes of the terminal O-W-O; and the band at 310 cm^{-1} belonged to the translational mode of simultaneous movement of Bi^{3+} and WO_6^{6-}.[10] Compared with pure Bi_2WO_6, new bands near 2100 cm^{-1} that could be ascribed to ferrocyanide was found for $K_4[Fe(CN)_6]$ treated Bi_2WO_6, and the bands in this wavelength range were intercepted for subsequently magnified analysis. The band at 2096 cm^{-1} corresponding to Eg mode of υ(C≡N) tensile vibration was included in both $K_4[Fe(CN)_6]$ treated Bi_2WO_6 and pure $K_4[Fe(CN)_6]$ samples, which belonged to N≡C-Fe, while the characteristic peak at 2124 cm^{-1} only appeared in the treated Bi_2WO_6 sample, which was ascribed to 1Ag+υ (C≡N) tensile vibration from the Bi-N≡C bond.[7]

From the FT-IR spectra (Fig. S4B), the Bi-O and O-W-O tensile vibrations of the untreated and treated Bi_2WO_6 samples were between 500 and 800 cm^{-1}.[11] And the two obvious absorption bands at 1630 and 3400 cm^{-1} were the tensile and bending vibration peaks of the –OH from adsorbed water molecules.[12] Compared with the untreated Bi_2WO_6, the –C≡N stretching vibration peak consistent with that of $K_4[Fe(CN)_6]$ appeared at 2045 cm^{-1}, confirming the successful coordination of hexacyanoferrate(II) on its surface.

As observed in Fig. S4C for the ultraviolet–visible diffuse reflectance spectra (UV–Vis DRS), the absorption of the Bi_2WO_6 was in the wavelength ranges of 200 to 420 nm. In contrast, the absorption ranges of $K_4[Fe(CN)_6]$ treated Bi_2WO_6 underwent a slight red shift, which was related to the formation of BiHCF on its surface. These absorption changes could also be observed by naked eye (insert image of Fig. 1D): bare Bi_2WO_6 sample was a white powder while the treated sample developed light yellow color.

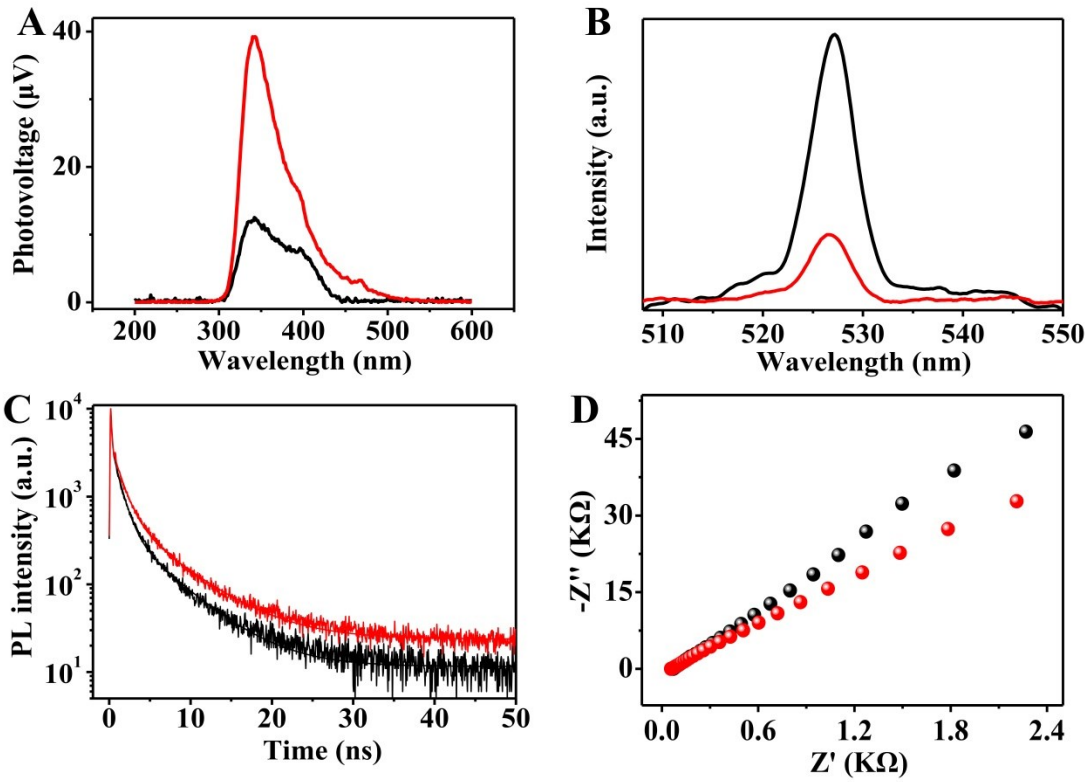

Fig. S5 The (A) SPV spectra, (B) fluorescence spectra, (C) time-resolved fluorescence spectra, and (D) Nyquist impedance plots of Bi_2WO_6 (black line) and $K_4[Fe(CN)_6]$ treated Bi_2WO_6 (red line). The impedance assays were conducted in 0.05 M Na_2SO_4 solution.

As shown in Fig. S5A, Bi_2WO_6 had a photovoltaic response in the 300–450 nm wavelength ranges, corresponding to its interband transition. In the similar wavelength ranges, the photovoltaic response of $K_4[Fe(CN)_6]$ treated Bi_2WO_6 increased significantly, indicating that the separation efficiency of photogenerated charge carriers inside the treated sample was greatly improved. The improvement in the efficiency of photogenerated carrier separation for treated Bi_2WO_6 was resulted from the formation of BiHCF on its surface. As shown in Fig. S5B, The FL spectral intensity of treated Bi_2WO_6 was lower than that of pure Bi_2WO_6, indicating that the migration efficiency of photogenerated charge carriers was improved for the treated sample, which was consistent with the SPV measurement.

Table S1 Kinetics of emission decay parameters of Bi_2WO_6 and $K_4[Fe(CN)_6]$ treated Bi_2WO_6 samples.

Sample	Component	Life time (ns)	B	B value	Relative percentage (%)
Bi_2WO_6	Γ_1	0.097	B_1	7371.8	10.82
	Γ_2	0.973	B_2	3484.9	51.02
	Γ_3	5.094	B_3	497.7	38.16
Treated Bi_2WO_6	Γ_1	0.082	B_1	7393.0	7.38
	Γ_2	1.178	B_2	3274.7	46.93
	Γ_3	5.733	B_3	655.4	45.69

$$(\tau) = \frac{B_1\tau_1^2 + B_2\tau_2^2 + B_3\tau_3^2}{B_1\tau_1 + B_2\tau_2 + B_3\tau_3} \quad \ldots\ldots(1)$$

The fluorescence lifetimes of the Bi_2WO_6 and $K_4[Fe(CN)_6]$ treated Bi_2WO_6 samples were calculated according to the above Equation (1).

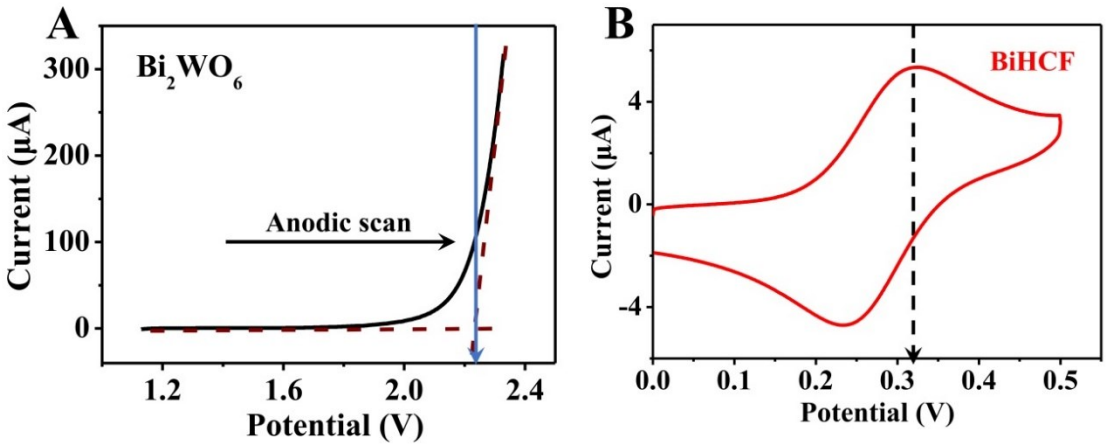

Fig. S6 (A) Anodic linear potential scan for determining the VB edge of Bi_2WO_6 in the deaerated Na_2SO_4 solution (0.2 M). (D) CV of BiHCF in the deaerated Tris-HCl solution (0.1 M, pH 7.0).

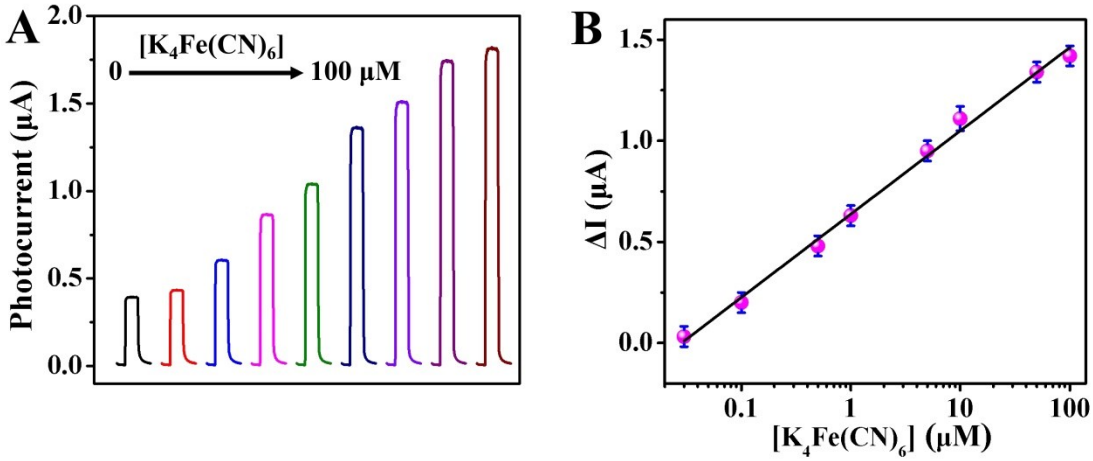

Fig. S7 (A) Photocurrent responses of Bi_2WO_6 electrode to different concentrations (from left to right, 0, 0.03, 0.1, 0.5, 1.0, 5.0, 10.0, 50.0, and 100.0 μM) of $K_4[Fe(CN)_6]$. (B) The corresponding linear curve.

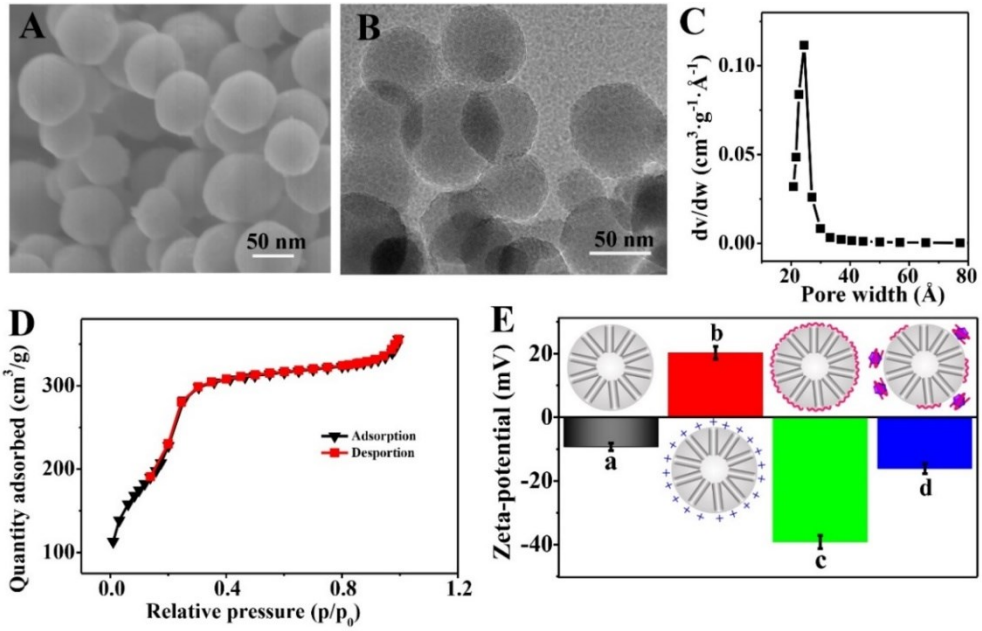

Fig. S8 (A) SEM image, (B) TEM image, (C) Pore size distribution, and (D) Nitrogen adsorption-desorption isotherms of MSN. (E) The Zeta potentials of MSN (a), PMSN (b), aptamer–capped PMSN (c), aptamer–capped PMSN after incubated with CAP (d).

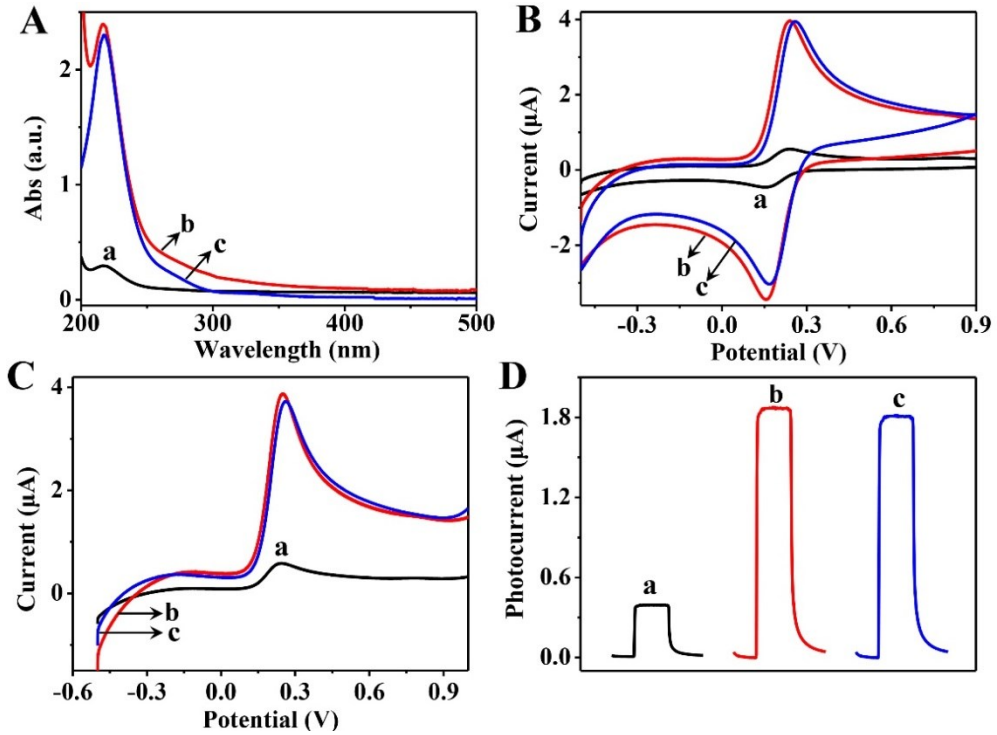

Fig. S9 The (A) UV-vis spectra of the supernatant, (B) CV curves, (C) LSV curves, and (D) photocurrent responses of the bioreaction systems when in the absence (a) and presence (b) of 0.1 μM CAP. A 0.1 mM $K_4[Fe(CN)_6]$ solution (c) was also used a control.

Table S2 Comparison with other reported methodologies for the detection of CAP.

Method	Material	Linear Range (nM)	LOD (pM)	Reference
Electrochemistry	———	1.6–4.2	1.6×10^3	13
Electrochemistry	p-AHNSA	$0.1–2.5\times10^3$	20.0	14
Electrochemistry	———	$1.0–1.0\times10^3$	2.9×10^2	15
Fluorescence	CdTe/GO	0.1–10.0	98.0	16
Photoelectrochemistry	Bi-BiOI@C	$2.0–2.5\times10^2$	7.9×10^2	17
Photoelectrochemistry	N-GQDs	$10.0–2.5\times10^2$	3.1×10^3	18
Photoelectrochemistry	Bi_2WO_6	5.0×10^{-2}-1.0×10^2	12.0	This work

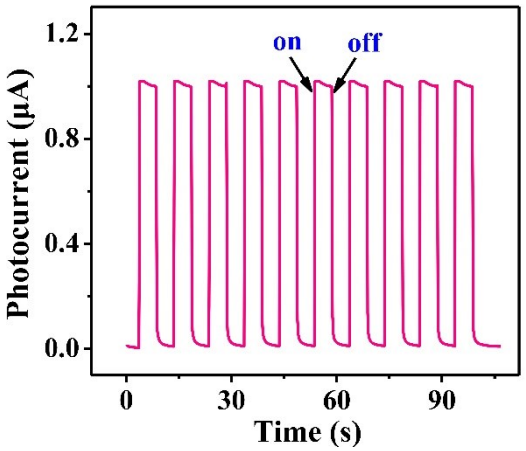

Fig. S10 Time dependent photocurrents of the proposed PEC detection system for 1.0 nM CAP under on−off irradiation repeats.

Table S3 The determination results of CAP in real samples (n = 5).

Sample	Added (nM)	Found (mean[a]±SD[b]) (nM)	Recovery (%)	RSD
River	0.00	0.00	/	/
	1.00	1.02±1.22	102.01	1.49
	10.00	9.89±1.31	99.24	2.23
	50.00	49.63±1.35	99.05	2.74
	75.00	75.81±1.04	101.12	1.37
Milk	0.00	0.00	/	/
	1.00	1.01±1.41	101.06	1.67
	10.00	10.12±0.53	101.11	1.58
	50.00	51.07±0.61	102.03	1.20
	75.00	74.73±1.47	99.63	1.96

Mean[a], the average value of five measurements. SD[b], standard deviation.

Reference

1 S. Luo, J. Ke, M. Yuan, Q. Zhang, P. Xie, L. Deng and S. Wang, *Appl. Catal. B-Environ.*, 2018, **221**, 215−222.

2 D. R. Radu, C. Y. Lai, K. Jeftinija, E. W. Rowe, S. Jeftinija and V. S. Y. Lin, *J. Am. Chem. Soc.*, 2004, **126**, 13216−13217.

3 P. Zhao, L. Cao, D. Ma, Z. Zhou, Q. Huang and C. Pan, *Nanoscale*, 2018, **10**, 1798−1806.

4 B. Zhang, B. Liu, J. Liao, G. Chen and D. Tang, *Anal. Chem*., 2013, **85**, 9245−9252.

5 C. Gao, J. Xue, L. Zhang, P. Zhao, K. Cui, S. Ge and J. Yu, *Biosens. Bioelectron*., 2019, **131**, 17−23.

6 S. B. Chen, H. Nan, X. Zhang, Y. T. Yan, Z. Zhou, Y. Zhang and K. Wang, *J. Mater. Chem. B*, 2017, **5**, 3718−3727.

7 W. O. Silva, V. C. Bassetto, D. Baster, M. Mensi, E. Oveisi, and H. H. Girault, *ACS Appl. Electron. Mater*., 2020, **2**, 927−935.

8 S. Su, X. Y. Han, Z. W. Lu, W. Liu, D. Zhu, J. Chao, C. H. Fan, L. H. Wang, S. P. Song, L. X. Weng and L. H. Wang, *ACS Appl. Mater. Interfaces*, 2017, **9**, 12773−12781.

9 Y. X. Zhao, Q. X. Lai, Y. Wang, J. J. Zhu and Y. Y. Liang, *ACS Appl. Mater. Interfaces*, 2017, **9**, 16178−16186.

10 B. Wang, L.P. Mei, Y. Ma, Y. T. Xu, S. W. Ren, J. T. Cao, Y. M. Liu and W. W. Zhao, *Anal. Chem*., 2018, **90**, 12347−12351.

11 Y. L. Tian, B. B. Chang, J. L. Lu, J. Fu, F. N. Xi and X. Q. Dong, *ACS Appl. Mater. Interfaces*, 2013, **5**, 7079−7085.

12 Z. J. Chen, Bi. Z. Lin, B. H. Xu, X. L. Li, Q. Q. Wang, K. Z. Zhang and M. C. Zhu, *J. Porous Mat*., 2011, **18**, 185−193.

13 S. Pilehvar, J. Mehta, F. Dardenne, J. Robbens, R. Blust and K. D. Wael, *Anal. Chem.*, 2012, **84**, 6753−6758.

14 S. K. Yadav, B. Agrawal, P Chandra and R. N. Goyal, *Biosens. Bioelectron*., 2014, **55**, 337−342.

15 L. Yan, C. Luo, W. Cheng, W. Mao, D. Zhang and S. Ding, *J. Electroanal. Chem*., 2012, **687**, 89−94.

16 M. Alibolandi, F. Hadizadeh, F. Vajhedin, K. Abnous and M. Ramezani, *Mater. Sci. Eng. C*, 2015, **48**, 611−619.

17 Y. Zhu, K. Yan, Z. Xu, J. Wu and J. Zhang, *Biosens. Bioelectron.*, 2019, **131**, 79−87.

18 Y. Liu, K. Yan, O. K. Okoth and J. Zhang, *Biosens. Bioelectron.*, 2015, **74**, 1016−1021.